

# Widening the Range of Trackable Environmental and Health Pollutants for Li-Garnet-Based Sensors

Moran Balaish and Jennifer L. M. Rupp\*

**Classic chemical sensors integrated in phones, vehicles, and industrial plants monitor the levels of humidity or carbonaceous/oxygen species to track environmental changes. Current projections for the next two decades indicate the strong need to increase the ability of sensors to sense a wider range of chemicals for future electronics not only to continue monitoring environmental changes but also to ensure the health and safety of humans. To achieve this goal, more chemical sensing principles and hardware must be developed. Here, a proof-of-principle for the specific electrochemistry, material selection, and design of a Li-garnet  $\text{Li}_7\text{La}_3\text{Zr}_2\text{O}_{12}$  (LLZO)-based electrochemical sensor is provided, targeting the highly corrosive environmental pollutant sulfur dioxide ( $\text{SO}_2$ ). This work extends the prime use of LLZO as a battery component as well as the range of trackable pollutants for potential future sensor-noses. Novel composite sensing-electrode designs using LLZO-based porous scaffolds are employed to define a high number of reaction sites, and successfully track  $\text{SO}_2$  at the dangerous levels of 0–10 ppm with close-to-theoretical  $\text{SO}_2$  sensitivity. The insights on the sensing electrochemistry, phase stability and sensing electrode/ $\text{Li}^+$  electrolyte structures provide first guidelines for future Li-garnet sensors to monitor a wider range of environmental pollutants and toxins.**

## 1. Introduction

### 1.1. Poor Air Quality: A Threat to Health and Climate

According to the World Health Organization (WHO), outdoor and household air pollution kill an estimated seven million people every year, accounting for one in eight deaths worldwide.<sup>[1]</sup> Ozone layer depletion (fluorocarbons, halocarbons), acid rain ( $\text{SO}_x$ ,  $\text{NO}_x$ ,  $\text{HCl}$ ), toxicity ( $\text{SO}_x$ ,  $\text{CO}$ ,  $\text{NO}_x$ ), and global warming (raising  $\text{CO}_2$ ,  $\text{CH}_4$ , fluorocarbon,  $\text{O}_3$  levels) are caused by numerous chemical pollutants emitted from diverse natural and industrial processes.<sup>[2,3]</sup> In the United

States, these contributors have led to an increased occurrence of natural disasters such as wild fires and hurricanes, which will continue to result in vast environmental climate-change-driven migration and resettling. As a consequence, disparities in terms of quality of life for humans will become much larger, demanding an affordable infrastructure that can locally measure changes in air pollution and minimize climate-change-induced socio-economic conflicts. Shifts in the local temperature, humidity, and pollutant levels can lead to new diseases and their spread, which in turn requires a careful understanding and measurement of the interplay between these processes. With roughly 91% of the world's population living in urban areas breathing polluted air,<sup>[1]</sup> solid-state sensors at relatively low cost for the monitoring and control of environmental quality are imperative to preserve air quality, human health, and the environment. In this context, sulfur oxides,  $\text{SO}_2$  and  $\text{SO}_3$ , make up a sizeable

portion of harmful pollutants, which are emitted from residential, manufacturing, and construction sectors through the combustion of sulfur-containing compounds in fossil fuels during oil and gas production and from natural processes such as volcanic eruptions and forest fires (Figure 1a).<sup>[4]</sup> Sulfur oxides may interact with the environment to cause toxicity, diseases, and environmental decay, playing a significant role in acid rain and having an adverse impact on forests, water, soil, corrosion, and human health (Figure 1b).<sup>[5–8]</sup> Moreover, considerable evidence indicates a link between  $\text{SO}_2$  exposure and risk of missed abortion in the first trimester of pregnancy, alongside higher likelihood of stillbirth and birth defects due to maternal long-term exposure to pollutants.<sup>[9,10]</sup> The permissible exposure limit to  $\text{SO}_2$  in the air and workplaces is 0.1–10 and 5 ppm, respectively, setting the upper limit for exposure without detrimental effects.<sup>[11,12]</sup> Conventionally,  $\text{SO}_2$  concentrations are measured using one of two optical tracking technologies, IR spectroscopy, or UV absorbance spectroscopy, which are accurate and stable but rather expensive and dependent on bulky instruments ( $\approx 50\ 000\ \text{cm}^3$ ) and thus not suitable for real-time continuous monitoring required in miniaturized applications (Figure 1c). Alternative detection methods include gas chromatography and flame emission spectrometry, which are expensive, time consuming, and demand high power and are thus impractical for real-time monitoring and feedback control on a daily basis.<sup>[11,13]</sup>

Dr. M. Balaish, Prof. J. L. M. Rupp  
Department of Materials Science and Engineering  
Massachusetts Institute of Technology  
77 Massachusetts Avenue, Cambridge, MA 02139, USA  
E-mail: jrupp@mit.edu

Prof. J. L. M. Rupp  
Department of Electrical Engineering and Computer Science  
Massachusetts Institute of Technology  
77 Massachusetts Avenue, Cambridge, MA 02139, USA

 The ORCID identification number(s) for the author(s) of this article can be found under <https://doi.org/10.1002/adma.202100314>.

DOI: 10.1002/adma.202100314

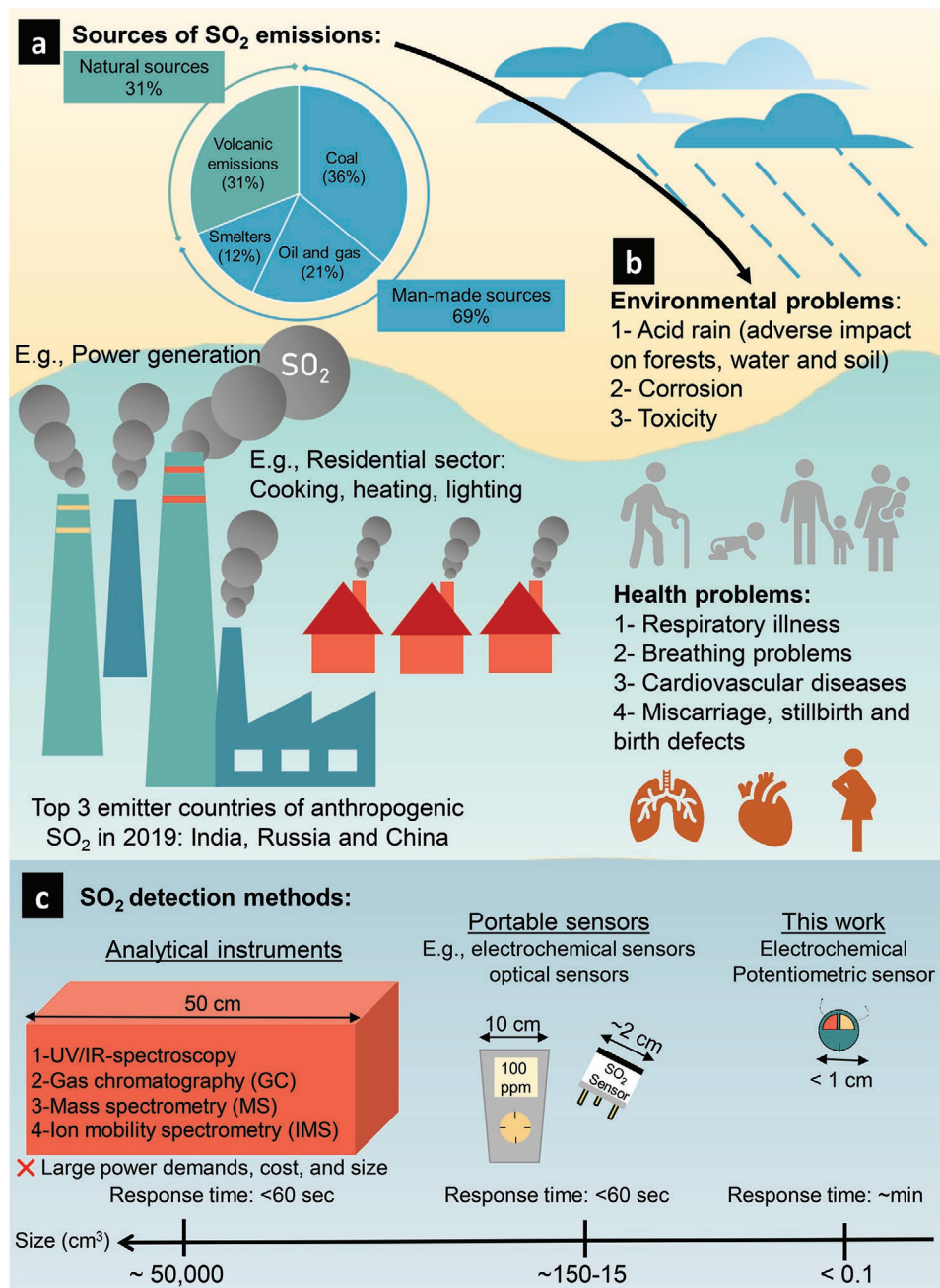


**Figure 1.** a–c) Schematic illustrations of natural and industrial sources of SO<sub>2</sub> emissions (a),<sup>[4]</sup> environmental and health problems associated with the emission of SO<sub>2</sub> polluters (b), and current detection methods of SO<sub>2</sub> gas (c).

## 1.2. Finding Room to Improve SO<sub>2</sub> Monitoring

In the quest to achieve continuous monitoring of harmful pollutants, solid-state resistive gas sensors employing semiconducting metal oxides (SMOX) have seen the widest spread in gas-sensing applications owing to their compactness and versatility.<sup>[14–16]</sup> The combination of their specific characteristics (e.g., physical, chemical, electrical, and thermal stability as well as corrosion resistance) alongside low thin-film processing costs for the integration of microarray sensors for multiple gas detection has positioned metal oxides as the most

advantageous materials for use in chemical sensors for applications in exhausts (500–1000 °C) or environmental monitoring (150–400 °C). For sensing of gaseous SO<sub>2</sub>, SMOX is typically composed of functional ceramics such as ZnO, CeO<sub>2</sub>, SnO<sub>2</sub>, Ga<sub>2</sub>O<sub>3</sub>, WO<sub>3</sub>, TiO<sub>2</sub>, or In<sub>2</sub>O<sub>3</sub>, which interact and exchange electrons with the targeted gas, yielding a change in the resistance of the metal oxide.<sup>[17–20]</sup> Resistive SMOX sensors can detect low gas concentrations with a fast response (typically around seconds), yet their selectivity is generally poor and unsatisfactory for practical applications. This poor selectivity stems from the operation of SMOX sensors being fully based on changes in

electrical resistance present rather than unspecific descriptors considering the possible adsorption of multiple gases.

The alternative to resistive sensing is to consider electrochemical gas sensors operating under thermodynamic equilibrium for the detection of CO<sub>2</sub>, SO<sub>2</sub>, and NO<sub>x</sub>. Such sensors employ ion-conducting solid electrolytes, where the conductivity stems from mobile ions rather than electrons, reducing susceptibility to corrosion and increasing selectivity, especially at low operation temperatures.<sup>[21]</sup>

### 1.3. Solid-State Electrochemical Gas Sensors

In a solid-state electrochemical gas sensor, a chemical gas species reacts at the electrode/ion-conductor interface where electrical charges are exchanged, resulting in an electrical signal that is directly related to the concentration or partial pressure of the gas species. Sensors for which the output is an electromotive force (emf) are referred to as potentiometric sensors (or impedance/ampereometric sensors if the output is electrical current) and can be used to track a wide variety of gaseous species. In other words, potentiometric solid-state electrochemical SO<sub>2</sub> sensors offer a promising alternative to the inconvenient UV and IR methods (with large power demands, cost, and size) by simply measuring chemical quantities and transducing them into electrical signals that correspond to the concentration of a particular chemical species. Until now, the potentiometric configuration has been the most widely used owing to its simple structure and operation principle, avoiding the need for complex electronics and thus providing higher cost efficiency for a wide range of applications. The solid-state potentiometric gas sensors were classified by Weppner into three types,<sup>[22]</sup> where the ion species derived from the tracked gas coincide with either the mobile ion (type I), the immobile ion (type II), or neither the mobile nor immobile ion but, rather, other ion species through the auxiliary sensing electrode (type III). Compared to types I and II, type III potentiometric sensors allow the detection of complex gas species (CO<sub>2</sub>, NO<sub>2</sub>, SO<sub>2</sub>) through the use of an auxiliary sensing electrode and a fast-ion-conducting electrolyte, obviating the need for separate gas environments for the sensing electrode (SE) and reference electrode (RE) (Figure 2a). The inherent simplicity of the structure of type III solid-state potentiometric electrochemical gas sensors, which are commonly constructed by combining a solid ion-conductor electrolyte with an auxiliary sensing electrode and a reference electrode, in addition to the direct voltage readout and scope for miniaturization have positioned them as an attractive detection method for various gases.<sup>[23]</sup> The emf of the cell is determined by the chemical potentials established at the sensing ( $\mu_{\text{Li}}^{\text{SE}}$ ) and reference electrodes ( $\mu_{\text{Li}}^{\text{RE}}$ ). At thermodynamic equilibrium, the measured voltage across the cell ( $E$ ) is related to the partial pressure of the detected gas ( $p(\text{SO}_2)^{\text{SE}}$ ) according to the Nernst equation (Figure 2a). The most widely used solid-state electrolytes in electrochemical gas sensors are O<sup>2-</sup>-ion conductors including yttria-stabilized zirconia,<sup>[24]</sup> tungsten-stabilized bismuth oxide, samarium-doped ceria, and Na<sup>+</sup>-ion conductors such as sodium beta-alumina<sup>[25]</sup> and NASICON.<sup>[26]</sup> Nevertheless, the relatively low mobility of the ions (i.e., O<sup>2-</sup>, Na<sup>+</sup>) in the solid

electrolyte remains a challenge for sensor operation. Typically, it necessitates rather high operating temperatures above 500 °C to ensure sufficient ionic conductivity for the solid electrolyte, which dictates the sensor's response and recovery time (Figure 2b).

### 1.4. State-of-the-Art Electrochemically Tracking of SO<sub>2</sub>

Most conventional solid electrolytes include either alkali-metal sulfates,<sup>[45,46]</sup> Ag–beta-Al<sub>2</sub>O<sub>3</sub>,<sup>[37]</sup> Na–beta-alumina Na<sub>2</sub>O–Al<sub>2</sub>O<sub>3</sub>,<sup>[25]</sup> NASICON (Na<sub>3</sub>Zr<sub>2</sub>Si<sub>2</sub>PO<sub>12</sub>),<sup>[26]</sup> LISICON (Li<sub>14</sub>ZnGe<sub>4</sub>O<sub>16</sub>),<sup>[47]</sup> or yttria-stabilized zirconia (YSZ).<sup>[24,48]</sup> Historically, the use of solid electrolytes for the detection of SO<sub>2</sub> and/or SO<sub>3</sub> was first suggested by Gauthier et al. in 1977.<sup>[49,50]</sup> As no solid electrolyte is based on the conduction of pure SO<sub>4</sub><sup>2-</sup> ions, solid-state electrochemical SO<sub>2</sub> sensors are typically either type II based on sulfate-based solid electrolytes such as K<sub>2</sub>SO<sub>4</sub>, Na<sub>2</sub>SO<sub>4</sub>, Li<sub>2</sub>SO<sub>4</sub>, or Ag<sub>2</sub>SO<sub>4</sub> or type III based on Na<sup>+</sup> conductors with an auxiliary sensing electrode, where a thermodynamic equilibrium persists between the solid electrolyte (ion conductor), current collector (electron conductor), and gas phase.<sup>[51]</sup> The first type III electrochemical solid-state SO<sub>2</sub> sensor, reported in 1985 by Maruyama et al.,<sup>[31]</sup> was based on a Na<sup>+</sup>-ion conductor, namely NASICON, and a Na<sub>2</sub>SO<sub>4</sub> auxiliary sensing electrode operated at 776 °C. Later on, to mitigate the instability of NASICON under the SO<sub>2</sub> environment at high temperatures, NASICON was replaced by a MgO-stabilized zirconia solid electrolyte and Li<sub>2</sub>SO<sub>4</sub>–CaSO<sub>4</sub>-based auxiliary sensing electrode.<sup>[36]</sup> The sensor operated at 650 °C in the range of 2–200 ppm (>10 ppm SO<sub>2</sub> concentration step) with a response/recovery time of 8–15 s/6–8 min by combining an anion-conducting solid electrolyte (O<sup>2-</sup>) with a cation-conducting auxiliary sensing electrode (Li<sup>+</sup>), imposing the formation of an ionic bridge interphase layer at the anion–cation conductor heterojunction interface to achieve an electrochemical chain. More recently, Ma et al. reported a mixed-potential SO<sub>2</sub> gas sensor using a NASICON solid electrolyte and orthoferrite (La<sub>0.5</sub>Sm<sub>0.5</sub>FeO<sub>3</sub>) as the sensing electrode and catalyst, respectively, to track sub-ppm levels of SO<sub>2</sub> (0.2–5 ppm) with a sensitivity of 86 mV per decade at 275 °C; however, data on response and recovery times stimulates follow-up work (Figure 2b).<sup>[27]</sup>

Practical commercial sensors for the detection of SO<sub>x</sub> typically operate above 500 °C and require relatively high power because of the following drawbacks: i) sluggish detection and regeneration of the sensor, originating from slow diffusion processes and insufficient oxygen-ion conductance in zirconia-based electrolytes ( $\approx 10^{-8}$  S cm<sup>-1</sup> at 300 °C) and poor ionic conductivity in NASICON ( $\approx 10^{-7}$  S cm<sup>-1</sup> at room temperature), resulting in limited speed of the electrode reaction and poor detection and/or response time (typically  $>= 5$  min) of the sensor with even longer recovery times (not always available/reported)<sup>[34,47,52–54]</sup> and ii) low chemical stability of the electrolyte, causing unstable voltage response as well as poor reproducibility and long-term stability. Although research has been mainly focused on type III electrochemical sensors for SO<sub>2</sub> using a NASICON solid electrolyte with fair to good response, drawbacks associated with stability and transport issues require research attention.

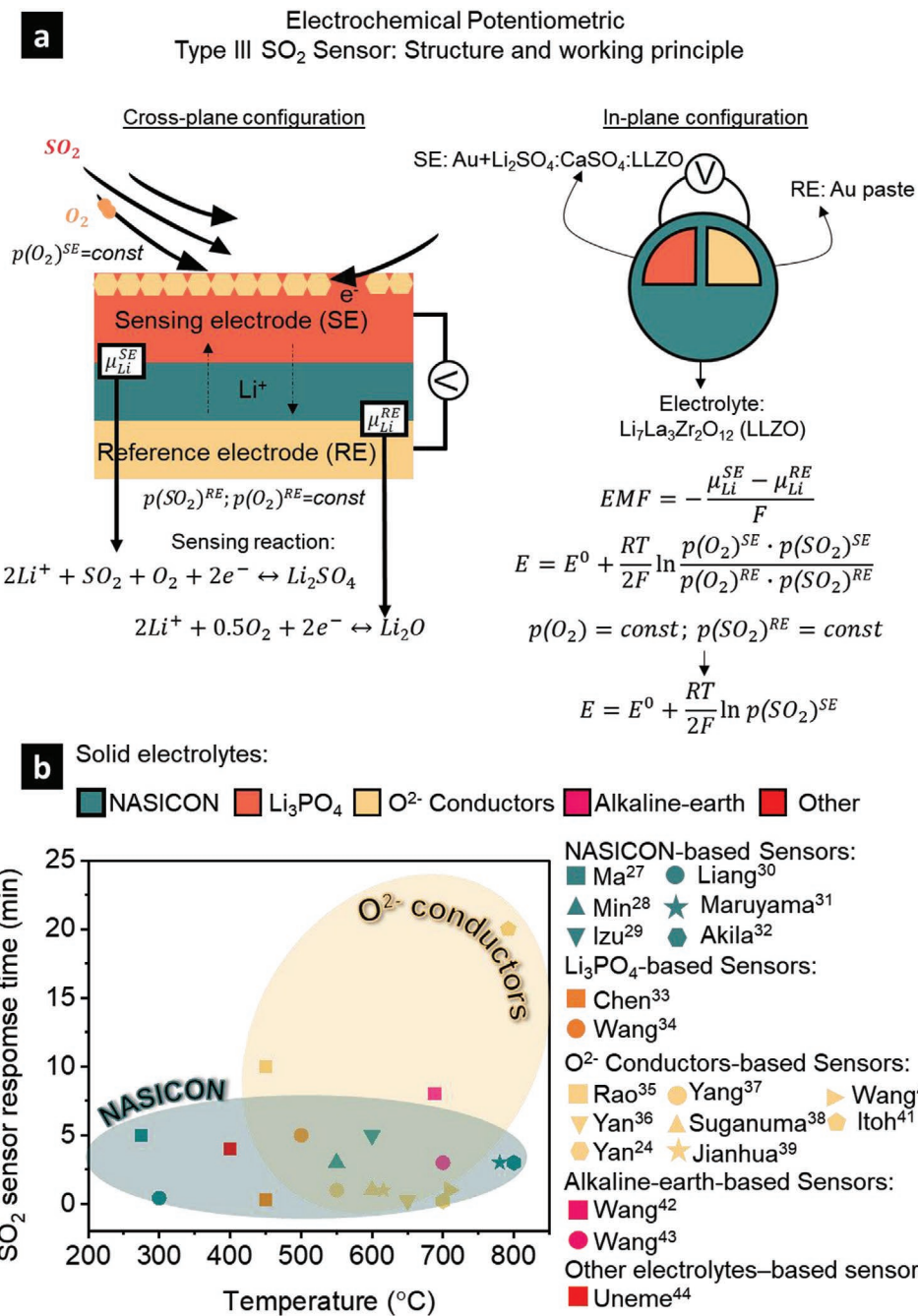


**Figure 2.** a) Sensing principles of type III potentiometric sensor tracking  $\text{SO}_2$  based on  $\text{Li}^+$ -based solid electrolyte, auxiliary sensing electrode, and gold (Au) reference electrode. The chemical gas species  $\text{SO}_2$  reacts at the electrode/ion conductor interface, where electric charges are exchanged, resulting in an electric signal that is directly related to the concentration or partial pressure of the gas species according to the Nernst equation. EMF is the electromotive force of the cell,  $\mu_{\text{Li}^+}$  is the chemical potential of  $\text{Li}^+$  at the sensing electrode or reference electrode, and  $F$  is the Faraday constant. b) Response time of  $\text{SO}_2$  potentiometric type III sensors based on typical solid electrolytes as a function of the operating temperature based on information in the literature: Ma et al.,<sup>[27]</sup> Min and Choi,<sup>[28]</sup> Izu et al.,<sup>[29]</sup> Liang et al.,<sup>[30]</sup> Maruyama et al.,<sup>[31]</sup> Akila and Jacob,<sup>[32]</sup> Chen et al.,<sup>[33]</sup> Wang et al.,<sup>[34]</sup> Rao et al.,<sup>[35]</sup> Yan et al.,<sup>[36]</sup> Yan et al.,<sup>[24]</sup> Yang et al.,<sup>[37]</sup> Suganuma et al.,<sup>[38]</sup> Yang et al.,<sup>[39]</sup> Wang et al.,<sup>[40]</sup> Itoh et al.,<sup>[41]</sup> Wang and Kumar,<sup>[42]</sup> Wang and Kumar,<sup>[43]</sup> and Uneme et al.<sup>[44]</sup>

### 1.5. Developing Environmental Sensors Based on $\text{Li}_7\text{La}_3\text{Zr}_2\text{O}_{12}$ Solid Electrolyte

There has always been a strong tie between the material development of solid electrolytes for solid-state batteries (SSBs) and

that for type III sensor applications, which is reviewed in more techno-historical detail in ref. [23]. After their discovery, Li solid-state electrolytes were mostly first integrated in solid-state batteries, with their integration in sensors lagging behind.<sup>[23]</sup> In some sense, the philosophy in the quest for an ideal ionic

solid is the same, with stable and highest ionic conduction for either fast charging in the battery or fast sensor response being sought. Where the philosophy differs in is the sensing and stability requirement under much harsher gas and temperature environments. For instance, the Li-garnet  $\text{Li}_7\text{La}_3\text{Zr}_2\text{O}_{12}$  (LLZO) is considered one of the promising solid electrolytes to be integrated in Li-metal-based SSBs considering its high room-temperature ionic conductivity ( $\approx \text{mS cm}^{-1}$  for the cubic phase), high chemical stability toward Li metal (reduction potential of 0.05 V vs  $\text{Li}^+/\text{Li}$ ), and wide electrochemical stability window.<sup>[55,56]</sup> Hence, it is not surprising that with the discovery of fast Li-garnet conductors as solid electrolytes for batteries, the idea for their integration in sensors to accelerate tracking of  $\text{CO}_2$  soon followed.<sup>[57,58]</sup> Moreover, prior theoretical and experimental studies of LLZO stability toward humidity and  $\text{CO}_2$  exposure<sup>[59,60]</sup> served as fertile ground for the development of LLZO-based sensors tracking  $\text{CO}_2$ . In 2018,  $\text{Li}_{6.75}\text{La}_3\text{Zr}_{1.5}\text{Ta}_{0.25}\text{O}_{12}$  was newly employed as a Li electrolyte for a type III potentiometric electrochemical sensor, creating a potential between a gold reference electrode and  $\text{Li}_2\text{CO}_3$  sensing electrode to track  $\text{CO}_2$ .<sup>[58]</sup> The sensors offered a fast response time of  $<60$  s at the lowered operation temperature of  $\approx 320$  °C, tracking 400–4000 ppm levels of  $\text{CO}_2$ .<sup>[58,61]</sup> These new sensing principles resulted in record-setting performance compared to that of state-of-the-art solid-state  $\text{CO}_2$  sensors based on solid-state ionic conductors and led to new use cases of classic battery Li electrolytes for the sensing field.<sup>[23,61]</sup> Nonetheless, whereas some properties of fast- $\text{Li}^+$ -conducting electrolytes may be more relevant for batteries, namely stability against Li metal, a wide electrochemical stability window, and favorable mechanical properties, solid-state electrochemical sensors require different requirements to operate well over the long term and differ clearly toward the well-established solid state electrolyte materials in batteries, see ref. [56] for detail. Primarily, investigation of the phase stability and transport properties upon prolonged exposure to the targeted gas and of the kinetic responses is needed. For instance, for battery operation in ambient conditions, a solid electrolyte may be targeted for  $10^5$  cycles and typical charge/discharge times of  $\approx 10$  h, whereas an electrochemical sensor operates continuously ( $\approx$ days) and requires response times on the order of seconds in a reducing gas environment. One may also add here, that recent discussion on the adaptability and processability of known battery solid state battery electrolytes from bulk (pellet or tape form) to thin film form for which we refer to ref. [62] has still to be translated to electrochemical gas sensors in future work as well. Given the potential to track  $\text{CO}_2$ , it is of high interest to expand the portfolio of LLZO-based sensors to also sense alternative pollutants; however, this possibility has not yet been explored. We see potential and express in this work that LLZO-based sensor hardware and its electrochemistry could be further developed for use in electronic noses, extending the range of trackable pollutants beyond  $\text{CO}_2$ , including new responses to corrosive  $\text{SO}_x$  environments and health threats.

This work provides a proof-of-principle for the electrochemistry, material selection, and design of  $\text{SO}_2$  sensing for Li-garnet conductors and contributes to the field in two ways. From a broader view, this work demonstrates the ability of fast SSB Li conductors of the garnet group to serve additional functionalities beyond battery components, and their potential to serve

as sensors not only for  $\text{CO}_2$  but now also for  $\text{SO}_2$  pollutants and health threats. Widening the spectrum of trackable pollutants to sulfur oxides and the intrinsically fast response times resulting from the fast-conducting solid  $\text{Li}^+$  electrolyte can serve as prerequisites for future sensor-nose technology and hardware in that area, which has not yet been expressed as an option. To succeed in proof-of-principle demonstration for  $\text{SO}_2$  sensing, it is imperative to first probe the material stability in the rather corrosive environment of  $\text{SO}_2$ , which has not yet been studied for Li-garnet conductors because of their prime use case as electrolytes in batteries. In addition, there has never been a material selection and design proposal for electrodes and their microstructure to access the newly proposed  $\text{SO}_2$  sensing electrochemistry, which we discuss and investigate in this work. Both are key to demonstrating whether such sensors can simply operate and to carefully discuss their characteristics in their response and recovery times and their sensitivity toward  $\text{SO}_2$  concentration step changes and optimal operation temperature ranges. Collectively, these are the first steps to expand the applications of a classic battery electrolyte to serve additional purposes with adapted electrochemistry and cell design to sense an extended range of pollutants from  $\text{CO}_2$  to  $\text{SO}_2$  for future devices.

## 2. Results and Discussion

### 2.1. Defining the Chemical and Thermal Stability Window of $\text{Li}_7\text{La}_3\text{Zr}_2\text{O}_{12}$ for $\text{SO}_2$ Environments

Future  $\text{SO}_2$  type III electrochemical sensors will require sufficient stability of the Li garnet electrolyte to maintain its phase and ensure sufficient Li conductivity to function for fast sensor response. To probe stability for the rather harsh environment, we fabricated dense and cubic Li-garnet solid-state electrolyte pellets ( $\text{Li}_{6.5}\text{La}_3\text{Zr}_{1.5}\text{Ta}_{0.5}\text{O}_{12}$ ) via classic solid-state synthesis (see Experimental Section and Figure S1, Supporting Information for SEM, XRD, Raman, and conductivity measurements of the unexposed pellets) and investigated their phase stability and microstructural changes when exposed to low and high  $\text{SO}_2$  concentrations of 4–250 ppm at temperatures between 240 and 480 °C for 24 h. In the following, we discuss morphological changes observed using SEM (Figure 3 and Figure S2, Supporting Information) and phase stability evaluated using both, XRD (Figure S3, Supporting Information) and Raman spectroscopy (Figure 4), to catch the potential changes in near-order vibration of the lattices in reaction to  $\text{SO}_2$  exposure.

#### 2.1.1. At Low $\text{SO}_2$ Concentrations (4 ppm)

The cubic garnet structure was maintained over the entire probed temperature range, 25–480 °C. At temperatures of 320 °C and above, the XRD peak signature at 22.23° became more prominent, which corresponds to (11̄1) diffraction of  $\text{Li}_2\text{SO}_4$ . We detected an increase in the thickness of the  $\text{Li}_2\text{SO}_4$  layer formed on LLZO from 0.5 to  $\approx 2$   $\mu\text{m}$  upon increasing the temperature from 240 to 480 °C, according to the SEM cross sections, Figure 3a (see also Figure S2, Supporting

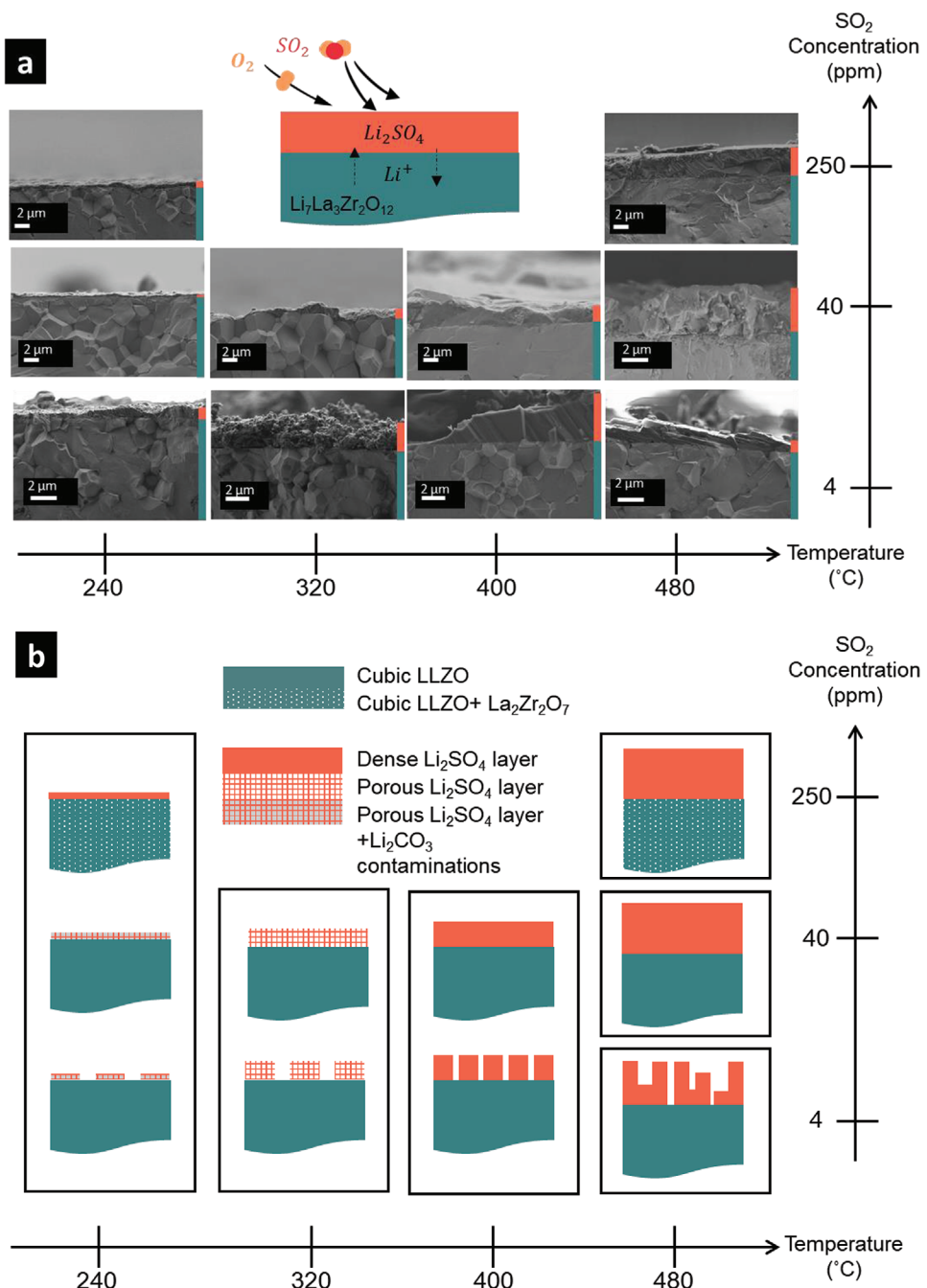


**Figure 3.** a) Cross-sectional SEM images of LLZO pellets after exposure to 4, 40, and 250 ppm  $\text{SO}_2$  at 240, 320, 400, and 480 °C for 24 h. The formation of  $\text{Li}_2\text{SO}_4$  was observed in all the studied cases. b) XRD characterization of the surface of the LLZO pellets after exposure to 4, 40, and 250 ppm  $\text{SO}_2$  at 240, 320, 400, and 480 °C for 24 h. In all the cases,  $\text{Li}_2\text{SO}_4$  was confirmed to be the main component of the surface layer and LLZO maintained its cubic phase. At high  $\text{SO}_2$  concentration (250 ppm), the formation of  $\text{La}_2\text{Zr}_2\text{O}_7$  was observed.

Information). For temperatures  $>320$  °C, a change in morphology from a continuous but porous layer of  $\text{Li}_2\text{SO}_4$  to a non-continuous and dense island-like layer was observed (Figure 3b). Although the formation of  $\text{Li}_2\text{SO}_4$  was likely enabled by the leaching of  $\text{Li}^+$  ions (presumably) from the surface of the LLZO pellet followed by a reaction with  $\text{SO}_2$  gas, its effect on the Li ionic conductivity of LLZO was found to be negligibly small, maintaining a conductivity of  $\approx 0.7 \text{ mS cm}^{-1}$

at ambient, and the cubic structure prevailed (Figure 4a and Figure S4, Supporting Information) when electrochemical impedance spectroscopy was used to estimate the bulk ionic conductivity of the same LLZO pellet after 24 h exposure to 10 ppm of  $\text{SO}_2$  at 240 and 480 °C (Figure S4, Supporting Information). Moreover, XPS analysis of pristine LLZO pellet and after 24 h exposure to 10 ppm of  $\text{SO}_2$  at 240 and 480 °C confirmed that sulfur was not incorporated in the LLZO

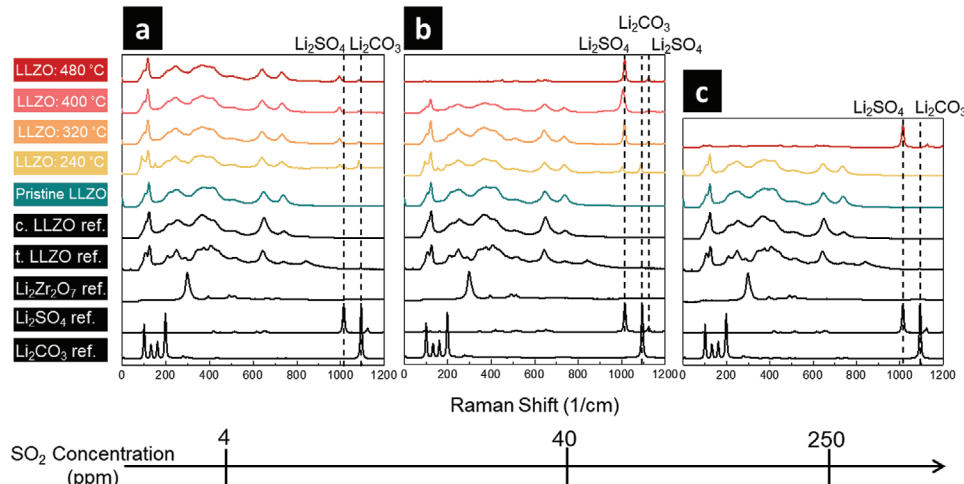


**Figure 4.** a–c) Raman spectra of LLZO pellets before (dark cyan) and after exposed to 4 ppm (a), 40 ppm (b), and 250 ppm (c) of  $\text{SO}_2$  at 240 °C (yellow), 320 °C (orange), 400 °C (pink), and 480 °C (red) for 24 h. In all cases  $\text{Li}_2\text{SO}_4$  was confirmed as the main component of the surface layer while LLZO maintained its cubic phase. At high  $\text{SO}_2$  concentration (250 ppm), the formation of  $\text{La}_2\text{Zr}_2\text{O}_7$  was observed. Additional reference spectra of  $\text{Li}_2\text{CO}_3$ ,  $\text{Li}_2\text{SO}_4$ ,  $\text{Li}_2\text{Zr}_2\text{O}_7$ , t. LLZO (tetragonal  $\text{Li}_{6.5}\text{La}_3\text{Ta}_{0.25}\text{Zr}_{1.5}\text{O}_{12}$ ), and c. LLZO (cubic  $\text{Li}_{6.5}\text{La}_3\text{Ta}_{0.25}\text{Zr}_{1.5}\text{O}_{12}$ ) are also displayed in black.

structure and only as a surface layer (Figure S5, Supporting Information).

#### 2.1.2. At Medium $\text{SO}_2$ Concentrations (40 ppm)

We observe the appearance of  $\text{Li}_2\text{SO}_4$  at roughly the same temperature threshold of 320 °C in the SEM, XRD, and Raman analyses, which is consistent with the observation of low  $\text{SO}_2$  concentration, Figure 3a and Figure S2 (Supporting Information). The thickness of the  $\text{Li}_2\text{SO}_4$  layer increased by one order of magnitude from ≈350 nm at 240 °C to ≈3.5 μm at 480 °C after exposure to 40 ppm  $\text{SO}_2$ . The top-view SEM images (Figure S2, Supporting Information) reveal more about the evolving growth of this layer starting from a porous morphology followed by an increase in grain size and densification of the  $\text{Li}_2\text{SO}_4$  layer as a function of temperature (Figure 3b). The complete coverage of the LLZO pellet by the dense  $\text{Li}_2\text{SO}_4$  layer aligns well with its principal observation in the Raman surface characterization (Figure 4b) and XRD bulk characterization (Figure S3, Supporting Information). These results were accompanied by a color change of the pellet from yellowish to white >400 °C.

#### 2.1.3. At High $\text{SO}_2$ Concentrations (250 ppm)

We exposed the LLZO pellets to rather harsh conditions during a 24-h period and probed the effect of temperature between 240 and 480 °C. Up to the tested 40 ppm  $\text{SO}_2$  exposure, we can confirm that the phase of the bulk LLZO did not change and remained cubic. At 250 ppm  $\text{SO}_2$ , XRD analysis (Figure S3, Supporting Information) revealed that even though the prime cubic phase remained LLZO, there was pronounced Li loss and the formation of lanthanum zirconate ( $\text{La}_2\text{Zr}_2\text{O}_7$ ), as indicated by the increasing intensity of the (111) diffraction peak at 28.5° with temperature (at both 240 and 480 °C). The cross-section (Figure 3a) and top-view (Figure S2, Supporting Information)

SEM images reveal a continuous and dense  $\text{Li}_2\text{SO}_4$  layer at 240 and 480 °C with thicknesses of ≈2.5 and 4 μm, respectively, exclusively covering the surface of the LLZO pellet (see SEM images, Figure 3a). Hence, we confirm that the cubic garnet structure was maintained as the majority phase up to 480 °C in the bulk; however, there is a threshold of ≈240 °C where in very harsh  $\text{SO}_2$  environments, Li leaches out from the garnet LLZO structure notably in the process of forming the  $\text{Li}_2\text{SO}_4$  surface layer (Figure 4c).

#### 2.2. Conclusions on Optimal Processing and Operation Range for a Li-Garnet $\text{SO}_2$ Sensor

Exploring the spontaneous formation and morphological evolution of  $\text{Li}_2\text{SO}_4$  under diverse  $\text{SO}_2$  concentrations and temperatures suggests that the major auxiliary sensing electrode component should preferably be  $\text{Li}_2\text{SO}_4$  to avoid its in situ formation during sensor operation and to better manipulate its morphology and thickness through the formation of an artificial sensing electrode layer. The thermodynamic (Supporting Information) and kinetic tendency for the formation of  $\text{Li}_2\text{SO}_4$  on LLZO at the investigated temperature and  $\text{SO}_2$  concentration range was confirmed. The latter is of high importance, indicating the feasibility of  $\text{SO}_2$  oxidation under the explored conditions, without the use of platinum (Pt) mesh (or other types of catalysts) typically employed to catalyze the oxidation of  $\text{SO}_2$ .<sup>[36]</sup> The investigation clarified that the  $\text{SO}_2$  concentration should be kept to <40 ppm, where the operation of the sensor at elevated temperatures (480 °C) could be realized without jeopardizing the cubic structure and high  $\text{Li}^+$  conductivity of LLZO, considering the potential long-term operation of the sensor.

Next, we wish to consider that once an artificial  $\text{Li}_2\text{SO}_4$  layer is introduced on top of the LLZO pellet as an auxiliary sensing electrode, the formation of a new  $\text{Li}_2\text{SO}_4$  layer, formed in situ on top of the LLZO layer during sensor operation, may be kinetically inhibited. To confirm or refute the last assumption,

additional stability investigation of garnet LLZO with an artificially deposited  $\text{Li}_2\text{SO}_4$  layer was executed. Qualitative analysis conducted using SEM images and elemental mapping (Figure S6, Supporting Information) of a LLZO pellet pre-deposited with  $\text{Li}_2\text{SO}_4$  and exposed to 10 ppm  $\text{SO}_2$  at 480 °C for 24 h revealed that the in situ formation of the  $\text{Li}_2\text{SO}_4$  layer was in fact inhibited. Thin (<500 nm) deposits (such as  $\text{Li}_2\text{CO}_3$  and  $\text{Li}_2\text{SO}_4$  deposits) were observed mainly at defected areas on the surface of the LLZO pellet. Moreover, as will be discussed in the following sections, post-mortem SEM and elemental mapping analysis of the sensing electrode/LLZO cross section revealed that the ≈15–20  $\mu\text{m}$ -thick sensing electrode remained unchanged throughout the sensing experiment (≈24 h) without the appearance of a new deposit layer on top of the sensing electrode.

The phase and microstructure evolution indicate that the processing range to first establish the sensing electrode formation of  $\text{Li}_2\text{SO}_4$  on LLZO are to be separated from the operation conditions of the sensor. i) Manufacture of the sensing electrode on LLZO pellets is best served artificially in a pre-fabrication step to operation, where its microstructure and composition can be tuned efficiently. ii) Operation of the  $\text{SO}_2$  sensor for LLZO should proceed at a lower temperature and  $\text{SO}_2$  level to keep the device steady and with low degradation. We conclude that the LLZO pellet remains primarily in the cubic phase, with no occurrence of the Li-loss phase observed for a critical amount of ≈3  $\mu\text{m}$  of  $\text{Li}_2\text{SO}_4$  formed when operated later between 240 and 480 °C for 4–40 ppm  $\text{SO}_2$ . Considering that the regulation values for  $\text{SO}_2$  detection in ambient atmosphere are 0.1–10 ppm and the stability analysis of Ta-doped  $\text{Li}_7\text{La}_3\text{Zr}_2\text{O}_{12}$  under diverse  $\text{SO}_2$  concentration and temperatures, the concentration of  $\text{SO}_2$  in this study was determined to be 0–10 ppm  $\text{SO}_2$ , for which we can assure phase stability of the LLZO pellet to serve later as an electrolyte and stability of the  $\text{Li}_2\text{SO}_4$  after formation. Based on these results, we targeted a temperature range of 240–480 °C to evaluate to the  $\text{SO}_2$  sensor performance and explore its effect on sensing.

### 2.3. Proof-of-Principle for Li-Garnet-Based $\text{SO}_2$ Sensors

As  $\text{SO}_2$  sensors based on  $\text{Li}_7\text{La}_3\text{Zr}_2\text{O}_{12}$  garnets do not yet exist, the electrochemical cell design and operational principles remain to be explored. In particular, the chemical stability of the sensing electrode/solid electrolyte requires careful analysis as the electrode/electrolyte interface plays a critical role in determining the performance characteristics of the gas sensor, which responds to the difference in the chemical potential of  $\text{Li}^+$  at the interfaces of the electrode. Utilizing a Li-garnet LLZO solid electrolyte with an “endless”  $\text{Li}^+$ -ion source of multiple cations that can easily diffuse to and from the auxiliary sensing electrode and chemically react either during the processing of the sensing electrode (750 °C) or during the operation of the sensor (480 °C) requires the exploration of the interplay between the auxiliary sensing electrode components and the Li-garnet solid electrolyte. It has been previously established that an auxiliary sensing electrode employing both  $\text{Li}_2\text{SO}_4$  and  $\text{CaSO}_4$  benefits from faster response time attributed to lower melting point and higher ionic conductivity of the two-component composite

electrode.<sup>[52,64,65]</sup> In the particular material composite case of  $\text{Li}_2\text{SO}_4\text{-CaSO}_4\text{|LLZO}$ , both the sensing electrode and the solid electrolyte are  $\text{Li}^+$ -ion conductors; explicitly,  $\text{Li}^+$  is the mobile ion. Thus, the electrochemical chain through the interface is simply achieved with  $\text{Li}^+$  ions. This is in contrast to type III potentiometric electrochemical sensors, where the sensing electrode and solid electrolyte are based on different mobile ions (e.g.,  $\text{Li}^+$  conductor and  $\text{O}^{2-}$  conductor for  $\text{Li}_2\text{SO}_4\text{|MSZ}$ ),<sup>[36]</sup> necessitating the formation of a mediating phase (ionic bridge) to provide a fast and stable electrochemical response by delivering a continuous path for ion conduction.<sup>[66–68]</sup> Nonetheless, the formation of an interfacial layer at the sensing electrode/solid electrolyte interface provided by interdiffusion and chemical reactivity, accelerated during heat treatment during the sensing electrode coating process (750 °C) or operation of the sensor (480 °C), may occur and deteriorate the  $\text{SO}_2$  sensing ability while establishing a complex voltage response due to competitive electrochemical reaction. Moreover, close inspection of the cross-sectional SEM images and elemental mapping of a sensor after a prolonged sensing experiment (Figure S7, Supporting Information) reveals an ≈1–2  $\mu\text{m}$ -thick Ca-rich layer sandwiched between the LLZO solid electrolyte and auxiliary sensing electrode.

To further investigate any possible chemical reaction between LLZO and the auxiliary sensing electrode ( $\text{Li}_2\text{SO}_4\text{-CaSO}_4$ ) and identify any reaction products that may have been formed during high-temperature heat treatment, powder mixtures of LLZO and sulfates at different mole ratios were heated at 750 °C for 2 h in oxygen, and compositional analysis was performed using XRD (Figure 5). The results indicated that once  $\text{CaSO}_4$  is exposed to heat treatment (either with or without

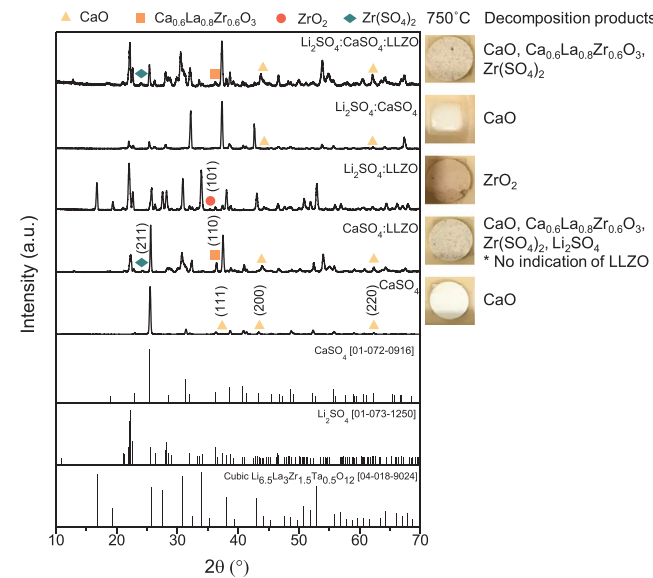


**Figure 5.** Chemical composition study of  $\text{CaSO}_4$ ,  $\text{Li}_2\text{SO}_4$ , and LLZO powders after they were compacted into model pellets and heat-treated at 750 °C for 2 h in oxygen. Once  $\text{CaSO}_4$  is exposed to elevated temperatures, the decomposition product  $\text{CaO}$  is formed. Once a mixture of  $\text{CaSO}_4$  and LLZO powders was exposed to 750 °C,  $\text{Li}_2\text{SO}_4$  was observed with no indication of LLZO.  $\text{CaO}$  [04-007-9734];  $\text{ZrO}_2$  [01-070-7358];  $\text{Ca}_{0.6}\text{La}_{0.8}\text{Zr}_{0.6}\text{O}_3$  [01-075-0354];  $\text{Zr}(\text{SO}_4)_2$  [00-024-1499].

$\text{Li}_2\text{SO}_4$ ), the decomposition product  $\text{CaO}$  is formed (followed by the evolution of  $\text{O}_2$  and  $\text{SO}_2$ ). Interestingly, for the  $\text{CaSO}_4$  and LLZO mixture, the decomposition products included not only  $\text{CaO}$  but also  $\text{Li}_2\text{SO}_4$  and  $\text{Ca}_{0.7}\text{La}_{0.6}\text{Zr}_{0.7}\text{O}_3$  compounds, yet no indication of LLZO was evident. In other words, once  $\text{CaSO}_4$  and LLZO were exposed to the typical heat treatment for a sensing electrode, the chemical reaction between the two components resulted in the complete consumption of the LLZO powder (or at least to the point where no LLZO was detected via XRD) and the formation of  $\text{Li}_2\text{SO}_4$ . To further corroborate the last finding,  $\text{CaSO}_4$  paste was brushed on an LLZO pristine pellet and heat treated at 750 °C for 2 h in oxygen. XRD analysis (Figure S8, Supporting Information) confirmed again the presence of  $\text{CaO}$ ,  $\text{Li}_2\text{SO}_4$ , and  $\text{CaSO}_4$  as decomposition reaction products and validated the formation of  $\text{Li}_2\text{SO}_4$  once a Li source (i.e., LLZO) and sulfate source (i.e.,  $\text{CaSO}_4$ ) are mixed together and heat treated. The results clarified that when using a Li-based solid electrolyte, although  $\text{CaSO}_4$  still assured the melting of the sensing electrode at lower temperature, securing good adhesion between the sensing electrode and solid electrolyte, its role as a humidity absorbent may have been diminished. Once the  $\text{Li}_2\text{SO}_4$  and LLZO mixture was heated, a decomposition product, possibly  $\text{ZrO}_2$ , was confirmed via XRD. However, the major decomposition products were evident once all three components, namely  $\text{Li}_2\text{SO}_4$ ,  $\text{CaSO}_4$ , and LLZO, were mixed together, confirming the chemical instability between the garnet LLZO solid electrolyte and the sensing electrode  $\text{Li}_2\text{SO}_4\text{--CaSO}_4$  during the heat-treatment procedure.

The lack of a stable interfacial compound or new decomposition products in the sensing electrode may account for the unstable behavior of the sensors and may require innovative auxiliary sensing electrode microstructure and composition design. Adding garnet LLZO to the auxiliary sensing electrode may further assist in both improving the ionic conductivity and response time of the sensor by: i) creating percolation pathways, where clusters with improved  $\text{Li}^+$ -ion conductivity through the use of LLZO are randomly connected; ii) increasing the effective surface area reaction by creating triple-phase boundary (TPB) reaction zones while shortening the  $\text{Li}^+$ -ion diffusion distance from the auxiliary sensing to the garnet LLZO solid electrolyte; and iii) stabilizing the solid electrolyte itself by playing an active role in forming an interfacial layer, thus helping to achieve thermodynamic equilibrium. Two main processing strategies were undertaken in order to incorporate garnet LLZO in the auxiliary phase ( $\text{Li}_2\text{SO}_4\text{--CaSO}_4$ ): i) LLZO calcinated powder was directly added to the sensing electrode paste followed by heat treatment at 750 °C and ii) a porous LLZO scaffold was created by preparing a porous LLZO layer on top of the LLZO sintered pellet,<sup>[63]</sup> followed by infiltration of the sensing electrode paste and subsequent heat treatment at 750 °C (see Experimental Section for detailed procedure).

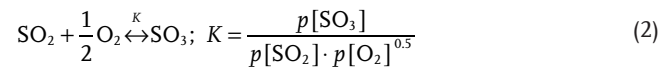
Following this design, the  $\text{SO}_2$  sensor was composed of the electrochemical cell expressed as



where gold (Au) is the reference electrode,  $\text{Li}_{6.54}\text{La}_{3.00}\text{Zr}_{1.36}\text{Ta}_{0.50}\text{O}_{11.73}$  is the solid electrolyte, and  $\text{Li}_2\text{SO}_4\text{--CaSO}_4\text{--LLZO}$  is the composite sensing electrode. When the cell

is heated to a stable thermal condition, mobile  $\text{Li}^+$  ions in the sensing electrode and the solid electrolyte can effectively take part in the electrochemical reaction, shifting it to an equilibrium state.

At the auxiliary sensing electrode, the oxidation of  $\text{SO}_2$  occurs according to the following reactions (Figure 2a):



$$\Delta G_f^0 = -97\,780 + 92.78 T [\text{K}] \quad (3)$$

where  $K$  and  $\Delta G_f^0$  are the equilibrium constant and the standard Gibbs free energy change in both reactions, respectively.<sup>[1]</sup> Thermodynamically, the oxidation of  $\text{SO}_2$  is feasible at room temperature and up to 780 °C. The overall reaction at the sensing electrode is expressed by,



At the reference electrode,  $\text{Li}^+$  ions are expected to react mainly with oxygen and not sulfur dioxide, possibly according to the following equation:



Considering that: i) the temperature and the partial pressure of  $\text{O}_2$  ( $p[\text{O}_2]$ ) are fixed in our current measurement set-up (0.21 atm) and ii) the activity of  $\text{Li}_2\text{SO}_4$  and  $\text{Li}_2\text{O}$  are kept constant and the concentration of  $\text{Li}^+$  is assumed to remain unchanged through the measurement, the cell potential (emf),  $E$ , is only determined by the partial pressure of  $\text{SO}_2$  ( $p[\text{SO}_2]$ ) according to the Nernst equation:

$$E = E^0 + \frac{RT}{2F} \ln(p[\text{SO}_2]) \quad (6)$$

where  $E^0$  is a constant (standard potential),  $F$  is the Faraday constant,  $R$  the gas constant, and  $T$  is the absolute temperature.

The electrochemical characterization of both devices to the  $\text{SO}_2$  response is depicted in Figures 6 and 7. In the case of the incorporation of a porous LLZO scaffold as a part of the sensing electrode (Figure 6a,b), a consistent increase in the emf of the sensor was observed in the electrochemical experiments measuring the emf response upon increase of  $\text{SO}_2$  concentration steps (Figure 6c). The response time was determined to be  $\geq 30$  min while the recovery time was achieved within  $\approx 4\text{--}15$  min. Nonetheless, the sensitivity of the sensor was determined to be 20.34 mV per decade ( $n = 7.3 e^-$ ) and 8 mV per decade ( $n = 18.6 e^-$ ) for the sensor response step (0–10 ppm) and recovery step (10–0 ppm), respectively, significantly lower than the theoretical sensitivity for a two-electron reaction of 74.64 mV per decade (Figure 6d). The poor sensitivity may imply that the in situ formation of  $\text{Li}_2\text{SO}_4$  is not kinetically favorable at the new auxiliary sensing electrode, and thus, we turn next to the second

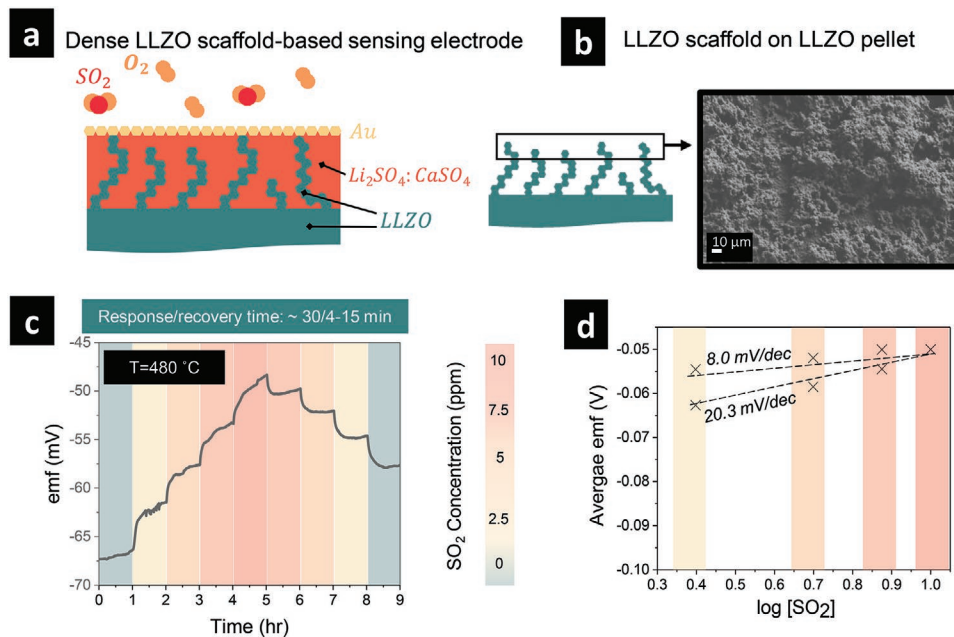


**Figure 6.** a) Schematic illustration of  $\text{SO}_2$  sensor with an LLZO-scaffold-based sensing electrode with a dense microstructure. b) Top-view SEM images of the LLZO scaffold on top of the LLZO pellet. c) Emf response to  $\text{SO}_2$  concentration step change (0–10 ppm) at 480 °C of the dense, LLZO-scaffold-based sensing electrode (recovery/response times are stated above and were extracted from the graphs). d) Emf dependence on the  $\text{SO}_2$  concentration on logarithmic scale showing sensitivity for dense, LLZO auxiliary sensing electrode.

alternative structure of the sensing electrode, that is, the composite sensing electrode. Once LLZO was added to the sensing electrode to create a dense composite electrode (Figure 7a,b), the sensitivity of the sensor was determined to be 48.4 mV per decade ( $n = 3.1 e^-$ ) and 42.9 mV per decade ( $n = 3.5 e^-$ ) for the sensor response step (0–10 ppm) and recovery step (10–0 ppm), respectively (Figure 7c,d). The response time of  $\geq 40$  min and recovery time of  $\geq 24$  min did not show improvement compared to those of the scaffold structure of LLZO (perhaps expected as a result of the less optimized network structure of the composite electrode); nevertheless, a complete recovery to the initial sensor voltage was achieved with similar sensitivity values upon increase and decrease of  $\text{SO}_2$  concentration steps (Figure 7d). In the composite structure where LLZO was distributed more homogeneously between the sulfate components and chemically reacted with them, the auxiliary sensing electrode was able to achieve for the first time in this study a new and stable thermodynamic equilibrium through both the response and recovery steps. The emf response of the electrochemical cells depicted in Figures 6a and 7a to  $\text{SO}_2$  concentration step at lower temperatures such as 240, 360, and 400 °C (not presented) did not show any meaningful response. Nonetheless, the most significant improvement in the response ability of the sensor was demonstrated for the composite sensing electrode by the operation of the sensor at significantly lower temperatures, namely 240 °C, which had not been achievable thus far for all the explored sensing electrode microstructures and compositions (Figure 7e). The response and recovery times of  $\geq 60$  min and  $\geq 4$  min, respectively, still require significant improvement, which may be achieved in the future by incorporating electronic conductors in the composite sensing electrode to meaningfully increase the active reaction zones. The sensitivity value was

determined to be 47.7 mV per decade ( $n = 2.1 e^-$ ) for the sensor response step (0–10 ppm), thus marking the auxiliary sensing electrode design as the first with a reported sensitivity value for the response reaction close to the theoretical value of 50.8 mV per decade (calculated for 240 °C) (Figure 8). It is hypothesized that lower operating temperature inhibits decomposition reactions between LLZO and  $\text{Li}_2\text{SO}_4$ – $\text{CaSO}_4$ , ensuring a sensitivity close to the theoretical value, implying thermodynamic equilibrium when using a composite sensing electrode. However, the lower operating temperature evidently has a significant effect on the  $\text{O}_2/\text{SO}_2$  desorption processes, decreasing the sensitivity to 8.2 mV per decade for the sensor recovery step (10–0 ppm), and may require the use of a catalyst to enable the operation of the sensor at such lower temperatures.

#### 2.4. Perspective on $\text{SO}_2$ Tracking and Sensor Design for Li-Garnet LLZO

The successful design of an electrochemical potentiometric type III sensor tracking  $\text{SO}_2$  necessitates the selection of materials in terms of chemistry and microstructure that provide a balance between an advantageous ion conductor, an auxiliary sensing electrode, and stable electrode/solid electrolyte interfaces, which play a critical role in determining the performance characteristics of the gas sensor. Most potentiometric type III  $\text{SO}_2$  sensors, are either based on  $\text{Na}^+$  conductors (NASICON),  $\text{O}^{2-}$  conductors (e.g.,  $\text{MgO}$ , beta-alumina),  $\text{Li}^+$  conductors ( $\text{Li}_3\text{PO}_4$ ), or other alkaline-earth-ion-conducting electrolytes (e.g.,  $\text{MgZr}_4(\text{PO}_4)_6$ ) in pellet, tube, or thick-film form, typically operate at higher temperatures (500–800 °C) with a response time that varies from  $\approx 1$  min to 20 min and characteristically

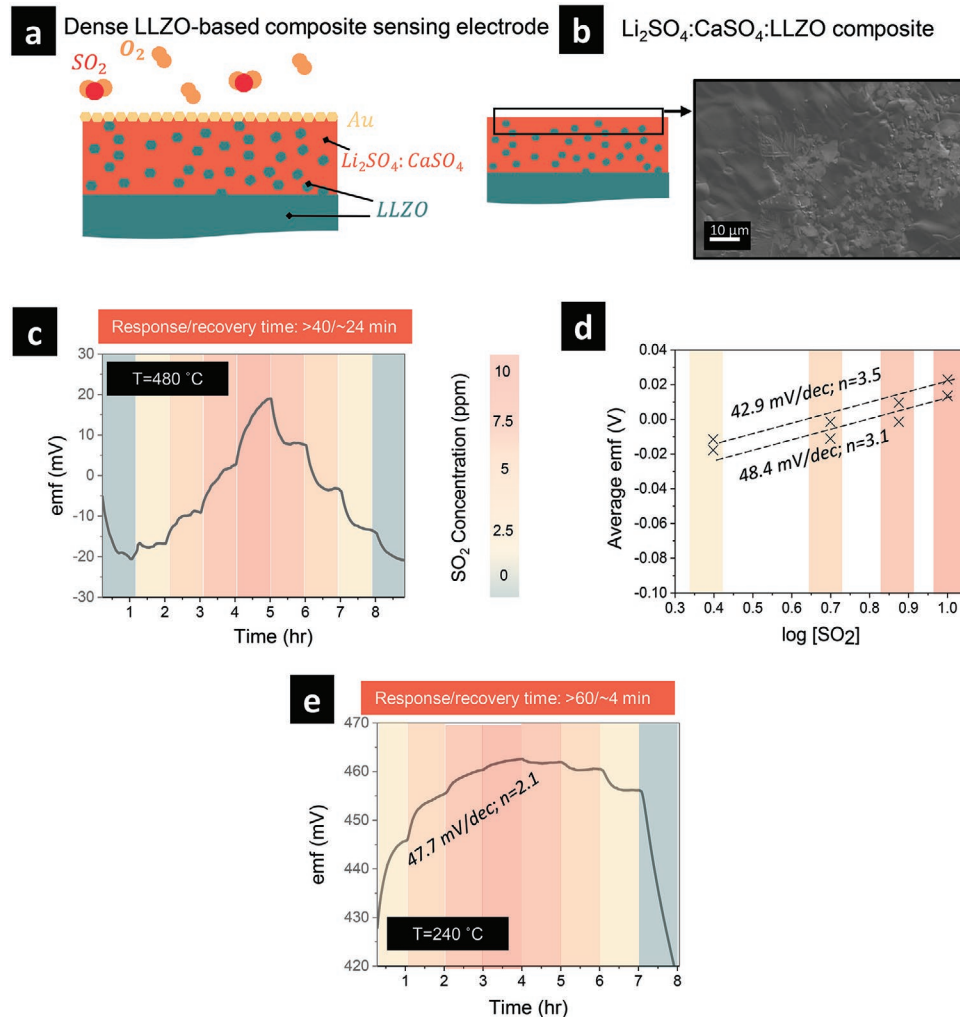


**Figure 7.** a) Schematic illustration of  $\text{SO}_2$  sensor with a dense LLZO-based composite sensing electrode microstructure. b) Top-view SEM images of the dense LLZO-based composite sensing electrode. c) Emf response to  $\text{SO}_2$  concentration step change (0–10 ppm) at  $480^\circ\text{C}$  of the sensor (recovery/response times are stated above and were extracted from the graphs). d) Emf dependence on the  $\text{SO}_2$  concentration on logarithmic scale showing sensitivity for the dense LLZO-based composite sensing electrode auxiliary sensing electrodes. e) Emf response to  $\text{SO}_2$  concentration step change (0–10 ppm) at  $240^\circ\text{C}$  of the dense LLZO-based composite sensing electrode (recovery/response times are stated above and were extracted from the graphs).

longer recovery times (Figure 2b) when compared to the composite-sensing-electrode-based sensor operated at  $240^\circ\text{C}$  at close-to-theoretical sensitivities presented here (Figure 8).<sup>[23]</sup> Moreover, most reported sensors track  $\text{SO}_2$  only in concentrations higher than 10 ppm toward hundreds and thousands of ppm of  $\text{SO}_2$ . Reported  $\text{SO}_2$  sensors covering similar  $\text{SO}_2$  concentration ranges tracked in this research typically operate at temperatures  $\geq 500^\circ\text{C}$ , except for a thick-film  $\text{SO}_2$  sensor based on NASICON solid electrolyte and  $\text{La}_x\text{Sm}_{1-x}\text{FeO}_3$  sensing electrode that has been reported to operate at  $275^\circ\text{C}$  but only to detect sub-ppm levels of  $\text{SO}_2$  (0.2–5 ppm).<sup>[27]</sup> Reported  $\text{SO}_2$  sensors operating at lower temperatures ( $400$ – $450^\circ\text{C}$ ) have shown sensitivity values that correlate with the calculated theoretical values or divert by up to  $\approx 20\%$ , with rather large spread in response times from  $\approx 18$  s to 10 min.<sup>[33,35,44]</sup> In addition, most type III electrochemical sensors detecting  $\text{SO}_2$  take advantage of the use of Pt (precious metal),  $\text{V}_2\text{O}_5$  (toxic), or  $\text{MgO}$  (serves

as a catalyst above  $300^\circ\text{C}$ )<sup>[69]</sup> as a part of the auxiliary sensing electrode (or as an external addition to catalyze  $\text{SO}_2$  oxidation) to effectively support fast  $\text{SO}_2$  oxidation in addition to  $\text{O}_2/\text{SO}_2$  adsorption and desorption processes and to significantly shorten the response/recovery time when the sensor is operated at lower temperatures. We wish to highlight that we have purposefully not taken advantage of any type of catalyst and focused on solely utilizing a fast ion conductor as a part of the sensing composite electrode and electrolyte to improve the diffusion process and reaction speed.

Indeed, Li-garnet LLZO has proven to show favorable thermodynamic and kinetic tendency for the formation of  $\text{Li}_2\text{SO}_4$  over a wide temperature range, without hampering the bulk ionic conductivity of the LLZO pellet through prolonged exposure to  $\text{SO}_2$ . We conclude, that Li-garnet can serve as a potentiometric electrochemical sensor tracking  $\text{SO}_2$  with a close-to-theoretical sensitivity at a remarkably low operation temperature

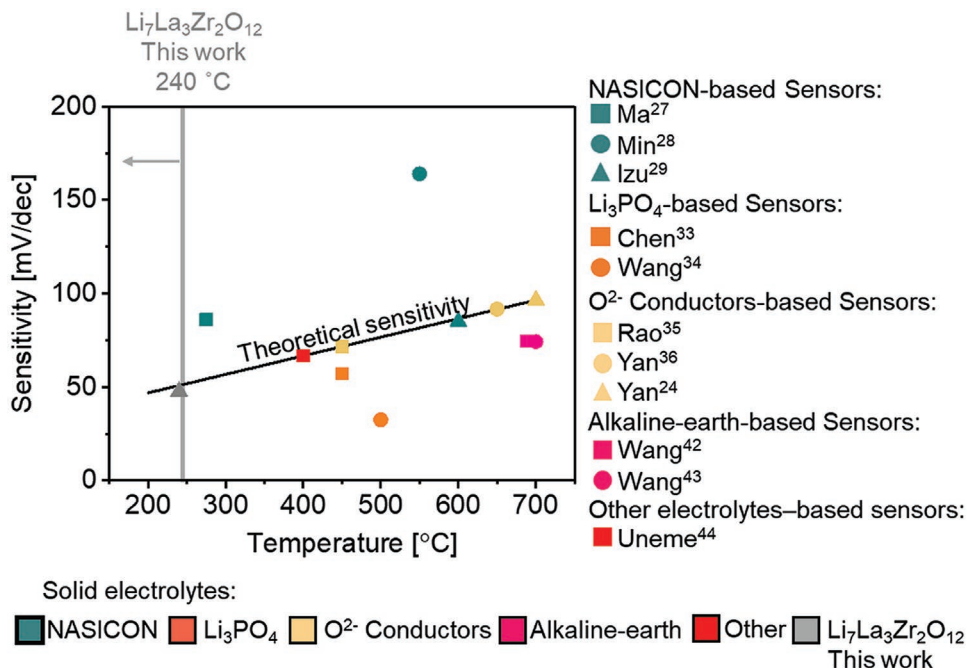


**Figure 8.** Comparison of the sensitivity (mV per decade) of SO<sub>2</sub> potentiometric sensors based on different solid-electrolyte types as a function of their operating temperature (°C).

of 240 °C (Figure 8) through the introduction of a composite sensing electrode (Li<sub>2</sub>SO<sub>4</sub>–CaSO<sub>4</sub>–LLZO). This sensing electrode design is expected to see wider success tracking other gases (e.g., CO<sub>2</sub>) without requiring an additional catalyst for the oxidation/reduction of the parent gas. We see perspective to further improve the response time for practical application in follow up work, for which one may envision novel porous sensing electrode architectures, inspired by the solid-state-battery field.<sup>[70]</sup> Alternatively, by using composite sensing electrode designs that are frequently used for SSBs (but have seen less exploration in the solid-state-sensor field), guidelines for the development of sensor tracking SO<sub>2</sub> (and other types of chemicals) based on a LLZO solid electrolyte can be further developed, contingent upon the introduction of a catalyst to secure fast gas oxidation and adsorption/desorption processes at low operating temperature with significantly inhibited electrolyte degradation. In addition, we highlight the importance of exploring the sensing electrode designs in future work to not only other gases such as H<sub>2</sub>O, H<sub>2</sub>S, NH<sub>3</sub>, and NO<sub>x</sub> but also to explore the cross-sensitivity and sensor response to other gases and impurities while detecting SO<sub>2</sub>.

### 3. Conclusion

Environmental sensors measuring a wide range of pollutants and toxins are essential in the early detection, real-time monitoring, systematic survey, analysis and simply for better management and safety of natural resources and humans. Particular interest is here to explore material classes and combinations thereof that may allow to measure not only a single pollutant but by a varied sensor electrode electrochemistry track a wide range of pollutants (e.g., CO<sub>2</sub>, SO<sub>2</sub>, NO<sub>2</sub>, and H<sub>2</sub>S). The critical

factors that determine the sensing performance for rather corrosive toxins such as SO<sub>2</sub> are to develop a suitable electrochemistry and sensor material selection stable in this environment, and operating at low temperature (ideally below 300 °C) to assure a low energy footprint per sensing device volume. One of the best investigated SO<sub>2</sub> electrochemical (type III) sensors are those based on the solid-state Na<sup>+</sup> conductor NASICON a known conductor vastly applied also as a battery solid state electrolyte. Despite the promise, the limited Na<sup>+</sup> conductivity at ambient around 10<sup>-7</sup> S cm<sup>-1</sup> challenges intrinsically to establish fast sensor response time and lower operation temperatures (energy footprint); which is also typically accompanied by degradation of the sensor performance and poor reproducibility. We propose in this work as a promising alternative cubic Li-garnet (LLZO) as a solid-state electrolyte for new SO<sub>2</sub> sensors due to their three orders of magnitude increased ionic conductivity ( $\sim$  mS cm<sup>-1</sup>) and higher electrochemical stability window, which allows a wider definition and choice for sensing material electrodes. The material class of Li-garnets is known for about a decade<sup>[23,62]</sup> and has proven success for solid state batteries, however, it had only recently been introduced to serve as electrolyte for type III sensors tracking less corrosive gases such as CO<sub>2</sub> with fast sensing and recovery times.<sup>[57,58]</sup> Looking ahead to widen potentially the spectrum of species that the material class of Li-garnet conductors can track for future type III sensors or noses, we envisioned through this work to learn how stable these are in corrosive environments, whether these are suited to create sensor electrochemistry dedicated to SO<sub>2</sub> and answering the fundamental question whether the 0 to 10 ppm limit of SO<sub>2</sub> can be tracked with reasonable performances to be meaningful for future environmental monitoring and analysis.

Taking key stability factors into account, such as making sure that the phase of the Li-garnet and conductivity are unchanged

during  $\text{SO}_2$  exposure of up to 10 ppm at maximum temperature of 480 °C, we could define functioning sensing devices based on  $\text{Li}_2\text{SO}_4\text{-CaSO}_4\text{-LLZO}$  composite sensing electrodes and Li-garnet solid electrolyte (LLZO) and prove their performance. For that, we explore the following sensor electrochemistry  $2\text{Li}^+ + \text{SO}_3 + \frac{1}{2}\text{O}_2 + 2e^- \leftrightarrow \text{Li}_2\text{SO}_4$  and investigated the major aspects that affect the electromotive force response according to the Nernstian behavior and the response/recovery time of the sensor, explicitly the auxiliary sensing electrode composition and microstructure. To assure a higher enough triple phase boundary, novel configurations, inspired by the battery field, were employed, namely composite designs of the auxiliary sensing electrode utilizing LLZO as a powder or porous scaffold. The  $\text{SO}_2$ -sensor operated at 480 °C with sensitivities ranging from 8 to 49 mV per decade and recovery/response times ranging from 4 to 60 min depending on the auxiliary sensing electrode configuration and  $\text{SO}_2$  concentration. The introduction of the composite sensing electrode  $\text{Li}_2\text{SO}_4\text{-CaSO}_4\text{-LLZO}$  with the LLZO electrolyte conductor achieved close-to-theoretical sensitivity of 477 mV per decade at remarkably low operating temperature of the sensor of 240 °C. We wish to highlight that this outperforms previously reported  $\text{SO}_2$  type III electrochemical sensors operating on  $\text{Zr}^{4+}$  (400 °C) or  $\text{Na}^+$  (600 °C) ion-conducting solid electrolytes in terms of their operation temperature and has as a consequence impact on the sensor power consumption (Figure 8).

This work demonstrates the ability to widen the functionalities of Li-garnet solid electrolytes beyond batteries and expands the spectra of trackable pollutants even under harsh environmental conditions from  $\text{CO}_2$  to now also  $\text{SO}_2$ . The material selection and design proposed for the electrodes and their microstructure unlocked the newly proposed  $\text{SO}_2$  sensing electrochemistry, which provides first guidelines for continuous, real-time monitoring of  $\text{SO}_2$  in practical applications. We foresee that the high phase stability and wide electrochemical stability window of Li-garnet electrolytes may serve many Lithionic<sup>[23]</sup> applications beyond batteries and in particular for future electrochemical sensor architectures. We envision that besides the known trackable  $\text{CO}_2$  pollutant, and now in this work added  $\text{SO}_2$ , also other pollutants such as  $\text{NO}_x$ , and  $\text{H}_2\text{S}$  may be suitable to be sensed with type III Li-garnet based electrochemical sensors in the future. Certainly, exploring the cross-sensitivity and sensor response to other gases, moisture and impurities while detecting  $\text{SO}_2$  remains to be explored and offers new research areas. We look ahead to see according sensor electrode material design and electrochemistry to-be-developed.

#### 4. Experimental Section

**Synthesis of LLZO Solid Electrolyte:** The solid electrolyte  $\text{Li}_{6.5}\text{La}_3\text{Zr}_{1.5}\text{Ta}_{0.5}\text{O}_{12}$  was prepared via solid-state synthesis using stoichiometric amounts of  $\text{La(OH)}_3$  (Sigma-Aldrich, 99.9%),  $\text{ZrO}_2$  (Sigma-Aldrich, 99.9%), and  $\text{Ta}_2\text{O}_5$  (Sigma-Aldrich, 99.99%) and an excess amount of 50 wt%  $\text{LiOH}$  (Alfa Aesar, purity 99.8%) to compensate for the lithium evaporation during the sintering process. The precursors were mixed and homogenized by planetary milling (PM, Across International, PQ-N04) in absolute isopropanol using  $\text{ZrO}_2$  balls for 1 h at 500 rpm and then dried at 90 °C. The obtained

powder was packed in the form of pellets, placed in  $\text{MgO}$  crucibles, and first-calcinated at 750 °C for 10 h at a heating rate of 5 °C min<sup>-1</sup> under the constant flow of synthetic air. Next, the powder was grinded and ball-milled in absolute isopropanol for another 12 h and then dried at 90 °C. The dried powder was second-calcinated at 750 °C in air for 5 h at a heating rate of 10 °C min<sup>-1</sup> under the constant flow of synthetic air. Finally, each ≈0.5 g of the powder was pressed into a pellet using a die with a diameter of 12 mm and thickness of 1.5 mm in a uniaxial press (2.2 tons cm<sup>-2</sup>). The green pellets were sintered in a  $\text{MgO}$  crucible under a constant flow of pure oxygen (50 sccm) at 1100 °C for 5 h at heating/cooling rates of 10 °C min<sup>-1</sup>. The sintered LLZO pellets were dry-polished to ensure consistency among all the samples. The chemical, thermal, and electrical characterizations of the pristine LLZO pellets are disclosed in detail in the Supporting Information.

**Fabrication of the Sensing Electrode and Sensor Device—Auxiliary (Sensing) Electrode:** The auxiliary electrode was prepared by mixing appropriate mole ratios of lithium sulfate ( $\text{Li}_2\text{SO}_4$ ; anhydrous, 99.99% trace metal basis, BeanTown Chemical) and calcium sulfate ( $\text{CaSO}_4$ ; anhydrous, 99.99% trace metal basis, BeanTown Chemical) with 10 wt% of the synthesized LLZO powder. A binder solution (mixture of  $\alpha$ -terpineol and ethylene cellulose) was added to the different ( $\text{Li}_2\text{SO}_4\text{:CaSO}_4$ ):LLZO powder mixtures in a weight ratio of 1:2; the resulting mixture was crushed and homogenized using a mortar until a smooth paste was produced. The paste was brushed on a quarter of the solid electrolyte and heated at 750 °C for 2 h at a heating rate of 10 °C min<sup>-1</sup> under the constant flow of pure oxygen (50 sccm). After the auxiliary (sensing) electrode preparation, a gold paste (Conductive Epoxy GOLD Paste, EMS) was brush-painted on the second quarter of the solid electrolyte surface, serving as the reference electrode (RE). A thin layer of the gold paste was brushed on the auxiliary (sensing) electrode, serving as a current collector. Platinum wires (0.1-mm diameter, 99.995%, BeanTown Chemical) were connected to the auxiliary (sensing) and reference electrodes using the gold paste. The complete sensor construction was annealed at 300 °C for 4 h in an oxygen atmosphere to cure the gold paste. An adhesive sealant was applied on the reference electrode (898FS, Cotronics Corp.) and cured again at 300 °C for 2 h in an oxygen atmosphere.

**Porous LLZO Scaffold Layer:** Inspired by the recent designs taken from the solid-state-battery field,<sup>[63]</sup> a porous LLZO layer was prepared by brushing a paste of the sintered LLZO powder and binder solution (mixture of  $\alpha$ -terpineol and ethylene cellulose) with a 1:1 weight ratio on top of the LLZO pellet. Corn starch (Sigma-Aldrich) was added as a pore former. The sample was sintered at 1100 °C for 2 h under oxygen flow. Once a porous LLZO scaffold was formed, a sensing electrode paste was sprayed on top of the porous LLZO and further heated to 750 °C for 2 h at a heating rate of 10 °C min<sup>-1</sup> under the constant flow (50 sccm) of oxygen.

**Spraying Procedure of the Sensing Electrode:** When better control of the thickness and geometry of the sensing electrode was required (for instance, in the case of the porous LLZO scaffold layer), a spraying procedure was employed. Appropriate amounts of the  $\text{Li}_2\text{SO}_4$  and  $\text{CaSO}_4$  powders were weighed and ball-milled in absolute isopropanol for another 3 h. The homogenized suspension was loaded into a spray gun (high-precision dual-action gravity feed airbrush, Gocheer) and sprayed on the LLZO pellet using a shadow mask. The sprayed sensing electrode was then heated at 750 °C for 2 h at a heating rate of 10 °C min<sup>-1</sup> under the constant flow (50 sccm) of pure oxygen.

**Chemical Stability Investigation of LLZO Solid Electrolyte and Auxiliary Sensing Electrode Components:** Powder mixtures of LLZO and the sulfates, i.e.,  $\text{LLZO:Li}_2\text{SO}_4\text{:CaSO}_4$ , in different mole ratios (namely 1:0:1, 1:1:2, 0:1:1, 1:0:0, 0:1:0, and 1:1:0) were thoroughly mixed using a mortar and pestle, packed into a 12-mm diameter die, and heated at 750 °C for 2 h at a heating rate of 10 °C min<sup>-1</sup> under the constant flow (50 sccm) of pure oxygen. The reaction products were identified using XRD.

**Sensing System Setup and Electrochemical Sensing Measurements:** The  $\text{SO}_2$  gas sensing experiments were conducted and measured using a Linkam stage (HFS600E) with an internal volume of ≈50 cm<sup>3</sup> equipped with a heating element in the temperature range of 25–600 °C. The

experimental set-up consisted of two automated mass flow controllers (red-y, Vogtlin Instruments, Switzerland) for 50 ppm SO<sub>2</sub> balanced by dry synthetic air and dry synthetic air (20% O<sub>2</sub> in N<sub>2</sub>). Reference humidity, ambient temperature, and SO<sub>2</sub> sensors (BW Clip SO<sub>2</sub> single gas detector, BW Technologies by Honeywell GasAlert Extreme Portable Sulfur Dioxide Monitor) were situated at the outlet of the measurement chamber. Different concentrations of the analyzed gas mixture, namely SO<sub>2</sub>, flown over the sensing electrode while maintaining a constant oxygen concentration of 20 vol%, were prepared by diluting 50 ppm of SO<sub>2</sub> balanced by synthetic air (20% O<sub>2</sub>, 80% N<sub>2</sub>) with dry synthetic air (20% O<sub>2</sub>, 80% N<sub>2</sub>) through a set of automated mass flow controllers (MFCs). The sensitivity of the sensor was evaluated through sensing experiments where the open-circuit voltage (OCV) was measured as a function of SO<sub>2</sub> concentration at a constant and calibrated temperature of either 240, 320, 400, or 480 °C at a heating/cooling rate of 10 °C min<sup>-1</sup>. The temperature calibration of the sensor was performed on the surface of the garnet LLZO pellet. The SO<sub>2</sub> profile was held with 2.5-ppm steps applied for 1–2 h in the range of 0–10 ppm SO<sub>2</sub>. The open-circuit voltage was measured using a Keithley 2612B electrometer. The reference and auxiliary (sensing) electrodes were contacted using the Pt wires, which were glued to the electrodes with gold paste.

**Surface and Bulk Characterization (EIS, SEM/EDS, In Situ/Ex Situ XRD, ICP, Raman)—Electrochemical Impedance Spectroscopy:** The electrical properties of the garnet LLZO solid electrolyte were investigated using impedance spectroscopy (VSP-300 potentiostat/galvanostat, Bio-Logic, Knoxville, TN, USA). The applied frequency range was 7 MHz to 1 Hz with a 20 mV AC amplitude. The LLZO sintered pellet was double-sided dry polished and subsequently covered with 150 nm Au electrodes by DC sputtering. The sample was placed in an air-tight T-cell.

**X-ray Diffraction:** XRD patterns of the solid electrolyte and the sensing electrodes were recorded using a Rigaku SmartLab diffractometer with Cu K $\alpha$  irradiation ( $\lambda = 1.5406 \text{ \AA}$ ). A step size of 0.01° and counting time of 3 s at 45 kV and 200 mA over the angular range of 10°–80° were used for the measurement.

**Inductively Coupled Plasma Mass Spectrometry:** The Li, La, Zr, and Al atomic compositions were determined by ICP-MS spectroscopy (Agilent 7900 ICP-MS) with an orthogonal detector system (ODS), which allows a wide dynamic concentration detection range from sub-ppt to percent-level concentration. Prior to the analysis and to avoid incorrect readings due to the formation of Li<sub>2</sub>CO<sub>3</sub> at the surface of the LLZO pellets, the samples were polished and a weighted amount was scraped off the sintered Ta-doped LLZO pellet and dissolved in aqua regia (36.5 wt% HCl 99.999% and 65–70 vol% HNO<sub>3</sub> 99.999%, trace metals basis, BeanTown Chemical) at 60 °C for 48 h in a closed vial to obtain clear solution. The solution was diluted immediately before the ICP-MS analysis. For internal standard purposes, 10 ppm Tb was used (10 ppm 3% v/v HNO<sub>3</sub>, Ricca Chemical Company) and calibration standard solutions were prepared from 10 ppm in 2% HNO<sub>3</sub> Li, La, Zr, and Al standards (Ricca Chemical Company) and diluted accordingly to prepare 0–10 ppm calibration standard solutions for each element. The ICP-MS results were normalized to the lanthanum and oxygen concentrations, estimated based on charge balance. The measurement was repeated at least 3 times.

**Raman:** The near-order characterization was performed using a confocal WITec alpha300 M+ Raman microscope (WITec, Germany) equipped with 532-nm excitation wavelength. All the Raman spectra were collected in ambient air.

**Scanning Electron Microscopy:** Field-emission scanning electron microscopes (FESEM Ultra Plus and FESEM Supra55VP equipped with an energy-dispersive X-ray spectrometer for elemental analysis and mapping, Zeiss) and a scanning electron microscope (SEM JEOL 7900F) equipped with a wide variety of detectors, including an EDS detector and a soft X-ray emission spectrometer (SXES) detector, allowed the efficient and parallel collection of very low-energy rays with chemical state analysis. The different scanning electron microscopes were employed to characterize the microstructure of the pristine LLZO pellets and complete sensor assemblies in addition to their post-mortem analysis after exposure to SO<sub>2</sub> at elevated temperatures.

## Supporting Information

Supporting Information is available from the Wiley Online Library or from the author.

## Acknowledgements

This work was supported in part by SENSE.nano under award number 2629303. M.B. acknowledges financial support from the US-Israel Fulbright Program, the Zuckerman Israeli Postdoctoral Scholar Program, and the MIT-Technion Postdoctoral Fellowship. J.L.M.R. thanks the Thomas Lord Foundation for financial support. This work made use of the MRSEC Shared Experimental Facilities at MIT, supported by the National Science Foundation under award number DMR-1419807. This work was performed in part at the Center for Nanoscale Systems (CNS), a member of the National Nanotechnology Coordinated Infrastructure Network (NNCI), supported by the National Science Foundation under NSF award no. 1541959. CNS is part of Harvard University.

## Conflict of Interest

The authors declare no conflict of interest.

## Author Contributions

M.B. and J.L.M.R. proposed the LLZO-based SO<sub>2</sub> sensor concept. M.B. proposed the sensor design, performed the experiments, and analyzed the results. M.B. and J.L.M.R. wrote the manuscript.

## Data Availability Statement

The data that support the findings of this study are available from the corresponding author upon reasonable request.

## Keywords

electrochemical sensors, Li garnet Li<sub>7</sub>La<sub>3</sub>Zr<sub>2</sub>O<sub>12</sub>, potentiometric sensors, SO<sub>2</sub> gas sensors

Received: January 13, 2021

Revised: February 6, 2021

Published online:

- [1] World Health Organization (WHO), "Ambient air pollution – a major threat to health and climate," can be found under, <https://www.who.int/airpollution/ambient/en/> (accessed: January 2021).
- [2] J. Hansen, M. Sato, P. Kharecha, G. Russell, D. W. Lea, M. Siddall, *Philos. Trans. R. Soc., A* **2007**, 365, 1925.
- [3] C. P. Chen, S. K. Tiong, S. P. Koh, F. Y. C. Albert, F. K. M. Yapandi, in *2018 3rd Int. Conf. Smart Sustain. Technol.*, **2018**, pp. 1–7.
- [4] S. Dahiya, A. Anhäuser, A. Farrow, H. Thieriot, A. Kumar, L. Myllyvirta, *Global SO<sub>2</sub> Emission Hotspot Database*, Center for Research on Energy and Clean Air & Greenpeace, Delhi, India **2020**, p. 48.
- [5] M. Kermani, S. Fallah Jokandan, M. Aghaei, F. Bahrami Asl, S. Karimzadeh, M. Dowlati, *Health Scope* **2016**, 5, e38736.
- [6] Y. Wu, R. Li, L. Cui, Y. Meng, H. Cheng, H. Fu, *Chemosphere* **2020**, 241, 125031.

- [7] G. Goudarzi, S. Geravandi, E. Idani, S. A. Hosseini, M. M. Baneshi, A. R. Yari, M. Vosoughi, S. Dobaradaran, S. Shirali, M. B. Marzooni, A. Ghomeishi, N. Alavi, S. S. Alavi, M. J. Mohammadi, *Environ. Sci. Pollut. Res.* **2016**, 23, 22001.
- [8] N. Greenberg, R. S. Carel, E. Derazne, A. Tiktinsky, D. Tzur, B. A. Portnov, *J. Toxicol. Environ. Health, Part A* **2017**, 80, 326.
- [9] L. Zhang, W. Liu, K. Hou, J. Lin, C. Zhou, X. Tong, Z. Wang, Y. Wang, Y. Jiang, Z. Wang, Y. Zheng, Y. Lan, S. Liu, *Nat. Sustain.* **2019**, 2, 1011.
- [10] S. Ha, R. Sundaram, M. B. Louis, C. Nobles, *Fertil. Steril.* **2018**, 109, 148.
- [11] D. D. Lee, *IEEE Sens. J.* **2001**, 1, 214.
- [12] Centers for Disease Control and Prevention (CDC), "NIOSH Pocket Guide to Chemical Hazards – Sulfur dioxide," can be found under <https://www.cdc.gov/niosh/npg/npgd0575.html> (accessed: January 2021).
- [13] Y. Liu, J. Parisi, X. Sun, Y. Lei, *J. Mater. Chem. A* **2014**, 2, 9919.
- [14] G. Korotcenkov, *Mater. Sci. Eng., B* **2007**, 139, 1.
- [15] M. K. Ram, *Sensors for Chemical and Biologocal Applications*, CRC Press/Taylor And Francis, Boca Raton, FL, USA **2010**.
- [16] K. Kalantar-zadeh, *Sensors: An Introductory Course*, Springer Science+Business Media, New York **2013**.
- [17] H. M. E. B. Várhegyi, J. Gerblinger, F. Réti, I. V. Perczel, *Sens. Actuators, B* **1995**, 25, 631.
- [18] D. Girardin, F. Berger, A. Chambaudet, R. Planade, *Sens. Actuators, B* **1997**, 43, 147.
- [19] F. Berger, M. Fromm, A. Chambaudet, R. Planade, *Sens. Actuators, B* **1997**, 45, 175.
- [20] Y. Shimizu, N. Matsunaga, T. Hyodo, M. Egashira, *Sens. Actuators, B* **2001**, 77, 35.
- [21] N. Miura, S. Yao, Y. Shimizu, N. Yamazoe, *Sens. Actuators B* **1992**, 9, 165.
- [22] W. Weppner, *Sens. Actuators* **1987**, 12, 107.
- [23] J. L. M. Zhu, Y. Gonzalez-Rosillo, J. C. Balaish, M. Hood, Z. D. Kim, K. J. Rupp, *Nat. Rev. Mater.* **2020**, <https://doi.org/10.1038/s41578-020-00261-0>.
- [24] Y. Yan, Y. Shimizu, N. Miura, N. Yamazoe, *Chem. Lett.* **1992**, 21, 635.
- [25] R. Akila, K. T. Jacob, *Sens. Actuators* **1989**, 16, 311.
- [26] S.-D. Choi, W.-Y. Chung, D.-D. Lee, *Sens. Actuators, B* **1996**, 36, 263.
- [27] C. Ma, X. Hao, X. Yang, X. Liang, F. Liu, T. Liu, C. Yang, H. Zhu, G. Lu, *Sens. Actuators, B* **2018**, 256, 648.
- [28] B. K. Min, S. D. Choi, *Sens. Actuators, B* **2003**, 93, 209.
- [29] N. Izu, G. Hagen, D. Schönauer, U. Röder-Roith, R. Moos, *J. Ceram. Soc. Jpn.* **2011**, 119, 687.
- [30] X. Liang, T. Zhong, B. Quan, B. Wang, H. Guan, *Sens. Actuators, B* **2008**, 134, 25.
- [31] T. Maruyama, Y. Saito, Y. Matsumoto, Y. Yano, *Solid State Ionics* **1985**, 17, 281.
- [32] R. Akila, K. Jacob, *J. Appl. Electrochem.* **1988**, 18, 245.
- [33] K. Chen, M. Zhang, H. Wang, H. Gu, *Rev. Sci. Instrum.* **2019**, 90, 065001.
- [34] H. Wang, Z. Liu, D. Chen, Z. Jiang, *Rev. Sci. Instrum.* **2015**, 86, 75007.
- [35] N. Rao, C. M. van den Bleek, J. Schoonman, O. T. Sørensen, *Solid State Ionics* **1992**, 53–56, 30.
- [36] Y. Yan, Y. Shimizu, N. Miura, N. Yamazoe, *Sens. Actuators, B* **1994**, 20, 81.
- [37] P. H. Yang, J. H. Yang, D. K. Peng, G. Y. Meng, *Soild State Ionics* **1996**, 86, 1095.
- [38] S. Suganuma, M. Watanabe, T. Kobayashi, S. I. Wakabayashi, *Solid State Ionics* **1999**, 126, 175.
- [39] J. Yang, P. Yang, G. Meng, *Sens. Actuators, B* **1996**, 31, 209.
- [40] L. Wang, R. V. Kumar, *Mater. Res. Bull.* **2005**, 40, 1802.
- [41] M. Itoh, E. Sugimoto, Z. Kozuka, *Trans. Jpn. Inst. Met.* **1984**, 25, 504.
- [42] L. Wang, R. V. Kumar, *J. Appl. Electrochem.* **2006**, 36, 173.
- [43] L. Wang, R. V. Kumar, *J. Electroanal. Chem.* **2003**, 543, 109.
- [44] Y. Uneme, S. Tamura, N. Imanaka, *J. Sens. Sens. Syst.* **2012**, 1, 29.
- [45] N. Imanaka, Y. Yamaguchi, G. Adachi, J. Shiokawa, *J. Electrochem. Soc.* **1987**, 134, 725.
- [46] G. Adachi, N. Imanaka, *Chem. Sens. Technol.* **1991**, 3, 131.
- [47] G. Jasinski, P. Jasinski, B. Chachulski, A. Nowakowski, *J. Eur. Ceram. Soc.* **2005**, 25, 2969.
- [48] F. Liu, Y. Y. Wang, B. Wang, X. Yang, Q. Wang, X. Liang, P. Sun, X. Chuai, Y. Y. Wang, G. Lu, *Sens. Actuators, B* **2017**, 238, 1024.
- [49] M. Gauthier, A. Chamberland, A. Belanger, M. Poirier, *J. Electrochem. Soc.* **1977**, 124, 1584.
- [50] M. Gauthier, A. Chamberland, *J. Electrochem. Soc.* **1977**, 124, 1579.
- [51] G. Korotcenkov, *Handbook of Gas Sensor Materials*, Springer, New York **2014**.
- [52] F. Ménil, B. O. Daddah, P. Tardy, H. Debéda, C. Lucat, *Sens. Actuators, B* **2005**, 107, 695.
- [53] G. Jasinski, P. Jasinski, B. Chachulski, A. Nowakowski, *Mater. Sci.* **2006**, 24, 261.
- [54] H. Wang, D. Chen, M. Zhang, J. Wang, *Surf. Coat. Technol.* **2017**, 320, 542.
- [55] R. Mahbub, K. Huang, Z. Jensen, Z. D. Hood, J. L. M. Rupp, E. A. Olivetti, *Electrochem. Commun.* **2020**, 121, 106860.
- [56] K. J. Kim, M. Balaish, M. Wadaguchi, L. Kong, J. L. M. Rupp, *Adv. Energy Mater.* **2020**, 11, 2002689.
- [57] Y. Zhu, V. Thangadurai, W. Weppner, *Sens. Actuators, B* **2013**, 176, 284.
- [58] M. Struzik, I. Garbayo, R. Pfenninger, J. L. M. Rupp, *Adv. Mater.* **2018**, 30, 1804098.
- [59] L. Cheng, E. J. Crumlin, W. Chen, R. Qiao, H. Hou, S. Franz Lux, V. Zorba, R. Russo, R. Kostecki, Z. Liu, K. Persson, W. Yang, J. Cabana, T. Richardson, G. Chen, M. Doeff, *Phys. Chem. Chem. Phys.* **2014**, 16, 18294.
- [60] A. Sharafi, S. Yu, M. Naguib, M. Lee, C. Ma, H. M. Meyer, J. Nanda, M. Chi, D. J. Siegel, J. Sakamoto, *J. Mater. Chem. A* **2017**, 5, 13475.
- [61] C.-M. Horejs, *Nat. Rev. Mater.* **2018**, 3, 41578.
- [62] M. Balaish, J. C. Gonzalez-Rosillo, K. J. Kim, Y. Zhu, J. D. Hood, J. L. M. Rupp, *Nat. Energy* **2021**, 6, 227.
- [63] K. J. Kim, J. L. M. Rupp, *Energy Environ. Sci.* **2020**, 13, 4930.
- [64] A. Lundén, K. Schroeder, H. Ljungmark, *Solid State Ionics* **1988**, 28–30, 262.
- [65] K. Singh, V. K. Deshpande, *Solid State Ionics* **1984**, 13, 157.
- [66] N. Ma, S. Ide, K. Suematsu, K. Watanabe, K. Shimane, *ACS Appl. Mater. Interfaces* **2020**, 12, 21515.
- [67] T. Kida, H. Kawate, K. Shimane, N. Miura, N. Yamazoe, *Solid State Ionics* **2000**, 136–137, 647.
- [68] Y. Yan, N. Miura, N. Yamazoe, *J. Electrochem. Soc.* **1996**, 143, 609.
- [69] J. H. Lunsford, *J. Catal.* **1972**, 26, 261.
- [70] G. T. Hitz, D. W. McOwen, L. Zhang, Z. Ma, Z. Fu, Y. Wen, Y. Gong, J. Dai, T. R. Hamann, L. Hu, E. D. Wachsman, *Mater. Today* **2019**, 22, 50.
- [71] M. Balaish, Z. D. Hood, J. L. M. Rupp, *US 63/154,336, 2021*.